

Stochastic-Robust Planning of Networked Hydrogen-Electrical Microgrids: A Study on Induced Refueling Demand

Xunhang Sun, *Graduate Student Member, IEEE*, Xiaoyu Cao, *Member, IEEE*, Bo Zeng, *Member, IEEE*, Qiaozhu Zhai, *Member, IEEE*, Tamer Başar, *Life Fellow, IEEE*, and Xiaohong Guan, *Life Fellow, IEEE*

Abstract—Hydrogen-electrical (HE) microgrids are increasingly assuming an important role on the pathway toward decarbonization of energy and transportation systems. This paper studies networked HE microgrids planning (NHEMP), considering a critical but often-overlooked issue, i.e., the demand-inducing effect (DIE) associated with infrastructure development decisions. Specifically, higher refueling capacities will attract more refueling demand of hydrogen-powered vehicles (HVs). To capture such interactions between investment decisions and induced refueling demand, we introduce a decision-dependent uncertainty (DDU) set and build a trilevel stochastic-robust formulation. The upper-level determines optimal investment strategies for HE microgrids, the lower-level optimizes the risk-aware operation schedules across a series of stochastic scenarios, and, for each scenario, the middle-level identifies the “worst” situation of refueling demand within an individual DDU set to ensure economic feasibility. Then, an adaptive and exact decomposition algorithm, based on Parametric Column-and-Constraint Generation (PC&CG), is customized and developed to address the computational challenge and to quantitatively analyze the impact of DIE. Case studies on an IEEE exemplary system validate the effectiveness of the proposed NHEMP model and the PC&CG algorithm. It is worth highlighting that DIE can make an important contribution to the economic benefits of NHEMP, yet its significance will gradually decrease when the main bottleneck transits to other system restrictions.

Index Terms—Microgrids planning, demand-inducing effect, decision-dependent uncertainty, parametric column-and-constraint generation, hydrogen-electricity synergy

NOMENCLATURE

Sets and Indices

(s, t)	Time index of operating period t in scenario s
Λ	Candidate node set for hydrogen-electrical (HE) microgrids
$\mathcal{C}(i)$	Set of children nodes of node i
$\mathcal{L}/(i, j)$	Set/index of distribution lines
$\mathcal{N}/i, j, l$	Set/index of nodes
S/s	Set/index of stochastic scenarios

This work was partially supported by the National Key Research and Development Program of China under Grant 2022YFA1004600, and by the National Natural Science Foundation of China under Grant 62373294, Grant 62192752, and Grant 62103321. (*Corresponding author: Xiaoyu Cao*)

Xunhang Sun, Xiaoyu Cao, Qiaozhu Zhai and Xiaohong Guan are with the School of Automation Science and Engineering, Xi'an Jiaotong University, Xi'an 710049, Shaanxi, China (e-mail: xhsun@sei.xjtu.edu.cn; cxykeven2019@xjtu.edu.cn; qzzhai@sei.xjtu.edu.cn; xhguan@xjtu.edu.cn).

Bo Zeng is with the Department of Industrial Engineering and the Department of Electrical and Computer Engineering, University of Pittsburgh, Pittsburgh, PA 15106 USA (e-mail: bzeng@pitt.edu).

Tamer Başar is with the Coordinated Science Laboratory, University of Illinois Urbana-Champaign, Urbana, IL 61801 USA (e-mail: basar1@illinois.edu).

\mathcal{T}/t	Set/index of operating periods
\mathcal{Z}/z	Set/index of refueling zones
Ω_{ess}	Set of Electrical storage system (ESSs)
Ω_{hss}	Set of Hydrogen storage system (HSSs)
Ω_{res}	Set of Renewable energy sources (RESs)
k	Index of candidate facilities
Parameters	
Δ_t	Time interval of operating period
$\delta_{k,i}^{s,t}$	Capacity time-varying factor of RES k restricted by natural resources at node i at (s, t)
$\eta_k^{\text{ch}}/\eta_k^{\text{dis}}$	Charge/discharge efficiency of ESS k
η_{elz}	Efficiency of electrolyzers
ι_{pl}	Penalty prices for unmet electric loads
\bar{E}_k	Unit energy capacity of component k in ESSs
$\bar{G}_{\text{pur},z}^t$	Hydrogen purchase limitation of zone z at t
\bar{P}_k	Unit capacity of component k
ϕ_{ht}	Dissipation factor of hydrogen tanks
π_s	Probability of scenario s
ρ_e^t/ρ_g	Retail electricity/hydrogen prices
σ	Scale factor from one typical day to one year
$\varphi_k^{\text{max}}/\varphi_k^{\text{min}}$	Max-/minimum power factor angle of RES k
$\varphi_{\text{pl},i}^{s,t}$	Power factor angle of electric loads at node i at (s, t)
q_{imp}^t/q_g^t	Utility prices for power/hydrogen procurement
$c_{\text{hem}}^{i\&m}/c_k^{i\&m}$	Annualized summation of investment cost and maintenance cost of HE microgrid/component k
DoD_k	Maximum depth of discharge of ESS k
LHV_{H_2}	Low heating value of hydrogen
$n_i^{\text{max}}/n_i^{\text{min}}$	Max-/minimum number of hydrogen dispensers (HDs) allowed to install at node i
$P_{k,\text{ch}}^{\text{max}}/P_{k,\text{dis}}^{\text{max}}$	Maximum charge/discharge power of ESS k
$PD_i^{s,t}$	Active electric loads at node i at (s, t)
r_{ij}/x_{ij}	Resistance/reactance of line (i, j)
$S_{\text{mv}}^{\text{max}}/S_{\text{lv},i}^{\text{max}}$	Capacity limit of medium/low-voltage substation
SR	Service rate of HD
$U_i^{\text{max}}/U_i^{\text{min}}$	Voltage magnitude upper/lower bound at node i
$x_{k,i}^{\text{max}}/x_{k,i}^{\text{min}}$	Max-/minimum number of component k allowed to install at node i
Variables	
$\xi_z^{s,t}$	Refueling demand of hydrogen-powered vehicles (HVs) at zone z at (s, t)
$fp_{ij}^{s,t}/fq_{ij}^{s,t}$	Active/reactive power flow on line (i, j) at (s, t)
$g_{\text{pur},i}^{s,t}$	Hydrogen purchased from market at node i at (s, t)
$gl_i^{s,t}/ul_{v,z}^{s,t}$	Met/unmet HV refueling demand at node i /zone z at (s, t)
$loh_{\text{ht},i}^{s,t}$	Level of hydrogen of hydrogen tanks at node i at (s, t)
n_i	Number of HDs at node i

$p_{mv}^{s,t}/q_{mv}^{s,t}$	Active/reactive power via medium-voltage substation at (s, t)
$p_{k,i}^{s,t}/q_{k,i}^{s,t}$	Active/reactive power output of RES k at node i at (s, t)
$p_{elz,i}^{s,t}/g_{elz,i}^{s,t}$	Power input/hydrogen outflow of electrolyzers at node i at (s, t)
$p_{lv,i}^{s,t}/q_{lv,i}^{s,t}$	Active/reactive power via low-voltage substation at node i at (s, t)
$pc_{k,i}^{s,t}/pd_{k,i}^{s,t}$	Charging/discharging power of ESS k at node i at (s, t)
$p_i^{s,t}/l_i^{s,t}$	Met/unmet electric loads at node i at (s, t)
$soc_{k,i}^{s,t}$	State of charge of ESS k at node i at (s, t)
$U_i^{s,t}$	Magnitude of voltage at node i at (s, t)
u_i	Binary, 1 if an HE microgrid is deployed at node i , and 0 otherwise
$x_{k,i}$	Number of component k at node i

I. INTRODUCTION

A. Background and Literature Review

ONLY by reaching global carbon neutrality in the middle of the 21st century can it be possible to control global warming within 1.5°C, thereby averting the extreme hazards caused by climate change [1]–[3]. To achieve carbon neutrality, it is imperative that the transportation sector, responsible for approximately 23% of social carbon emissions, undergoes a profound transformation towards the low-carbon paradigm [4]. Compared to carbon-intensive fossil-fuel vehicles, the hydrogen-powered vehicles (HVs) are garnering increasing public attention, owing to their advantages of zero carbon emissions [5], [6].

Meanwhile, the rapid proliferation of HVs raises enormous challenges to the energy sector for hydrogen supply. Traditionally, hydrogen is mainly produced via centralized fossil-based ways, e.g., steam methane reforming (SMR) and coal gasification (CG), and then stored and delivered to end-users through the hydrogen supply chain [7]–[9]. Although this procedure is profitable, these hydrogen production measures could come with a poor environmental impact attribute to inherent carbon emissions.

To support carbon-free hydrogen supply, it would be a viable approach to seek for dispersed generation of renewable energy sources (RESs) over the power distribution network (PDN), which is the critical infrastructure coupled with the urban transportation system. The interdependence facilities of RES generation, on-site hydrogen production and storage, as well as HVs' refueling can constitute a hydrogen-electrical (HE) microgrid for decarbonizing both the energy and transportation sectors [10]. In particular, HE microgrids exploit the "otherwise-curtailed" renewable electricity generated from wind and solar energy installations to produce hydrogen to supply HVs by means of the power-to-hydrogen (P2H) technology, i.e., water electrolysis. It is noteworthy to mention that such refueling procedure for HVs is carbon-free. On the other hand, the RES outputs could be effectively harnessed to support the flexible operation of PDN. Also, by incorporating the electrical and hydrogen storage systems, a clustering of HE

microgrids could actively participate in demand response (DR) programs, thereby enhancing their economic benefits [11].

Electrolytic production of hydrogen, however, suffers from high financial costs [12]. As mentioned in [8], the hydrogen cost of renewable electrolysis is 2.78-11.19 and 4.31-17.37 times higher than SMR and CG, respectively. Hence, a proper deployment of HE microgrids is crucial for meeting HV refueling demand and enhancing economic efficiency. The primary challenge of HE microgrids planning is the uncertain risks embedded in both the supply side (e.g., intermittent RES outputs) and the demand side (e.g., stochastic HV refueling demand and electric loads). How to make effective siting and sizing decisions for HE microgrids within highly uncertain environments is an important line of current research. Based on the statistical characteristics of uncertain risks, Ref. [10] has proposed a two-stage stochastic programming method for HE microgrids planning, using scenarios that capture the uncertainties. Furthermore, Ref. [13] has presented a multistage stochastic extension for systems' dynamic evolution, considering both the strategic and operating uncertainties under multiple timescales. Besides, Refs. [14]–[16] have exploited uncertainty sets to handle the uncertainties associated with HE microgrids operation, and then proposed planning methods based on robust optimization. Note that in these existing works, the risks are generally modeled as *decision-independent uncertainties (DIUs)*, or exogenous uncertainties [17], [18]. More specifically, the DIU factors are often assumed to demonstrate a fixed (static) nature of randomness, i.e., taking values according to a pre-defined stochastic distribution or an uncertainty set.

Practically, it is often the case that more constructions and capacities attract higher traffic or demand, a phenomenon referred to as *demand-inducing effect (DIE)* [19], [20]. In fact, DIE is quite relevant in planning and building transportation infrastructure. Ref. [21] has investigated the refueling station location problem, showing that without a DIE consideration, the planning scheme might result in a potential reduction of up to 17.07% in the serviced traffic flows. Ref. [22] has mentioned that a 10% increase in the number of public charging stations would increase the sales of electric vehicles by about 8%. In HE microgrids planning, it is also anticipated that the DIE, i.e., HV refueling demand would be induced by hydrogen refueling capacities, should be strong. Nevertheless, we note that the existing literature still lacks a systematic study.

Actually, the traditional DIU-based model cannot capture the system endogeneity (dynamics) associated with the DIE for HVs. In contrast, the *decision-dependent uncertainty (DDU)*, also known as endogenous uncertainty [17], [18], fits better into the description of refueling demand in this situation. Note that the planning schemes of HE microgrids without a DDU consideration are inadequate in handling the uneven demand distribution incurred by DIE, which would reduce the economic benefits. Therefore, in this study, we investigate the networked HE microgrids planning (NHMP) problem with the DDU modeling of HV refueling demand, to support the low-carbon and economic development of the synergistic energy-transportation system.

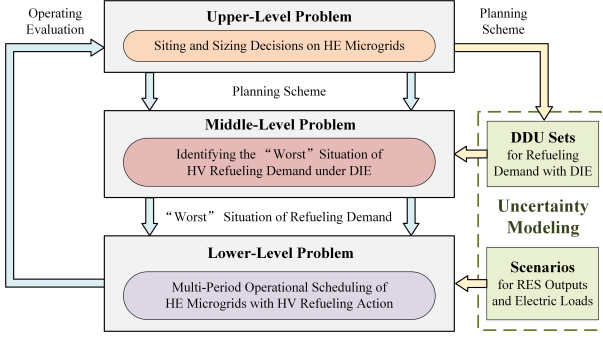


Fig. 1. Framework of trilevel stochastic-robust NHEMP problem.

B. Contribution and Paper Structure

This paper presents a stochastic-robust planning method for networked HE microgrids, taking DIE into consideration. To ensure the economic feasibility of NHEMP with respect to the uncertain future HV refueling demand, we adopt a trilevel min – max – min formulation that inherently embodies the idea of robust optimization. The upper-level problem determines the siting and sizing strategies for HE microgrids with minimum annual capital expenditures (CAPEXs) and maintenance costs. The middle-level identifies the “worst” situation of refueling demand by adopting DDU sets. The DDU sets can capture the influence of investment decisions to refueling demand, which analytically reflects the DIE. Then, in the lower-level problem, the multi-period operational schedule of HE microgrids associating with HV refueling actions is optimized to evaluate the profitability of the deployment scheme. Besides the DDU description, some other regular uncertain factors, i.e., the random variation of RES outputs and electric loads, are also considered in our NHEMP model by using a series of stochastic scenarios. In a summarized form, the decision framework is depicted in Fig. 1.

The resulting NHEMP formulation has *mutual interactions between investment strategies (upper-level decisions) and refueling demand (environment parameters in the middle-level)*. The popular Column-and-Constraint Generation (C&CG) algorithm [23] for classical DIU-based min – max – min problems cannot handle it because the DDU sets dynamically vary with the upper-level decisions. To address the computational intractability, we analyze the differences between the DDU and DIU sets, and derive a set of structural properties. Following them, an adaptive decomposition algorithm based on Parametric C&CG (PC&CG) is tailored and developed, which demonstrates a superior and exact solution capacity.

In comparison to existing literature, the contributions of this paper can be summarized as below:

- 1) The often-overlooked DIE is taken into consideration in the context of hydrogen-electrical microgrid planning, and the corresponding refueling demand is captured by a DDU set. Note that DIE, if exists, cannot be ignored as it can generate a critical impact in system planning. Also, our modeling scheme provides a rather general tool to investigate DIE in other practical systems.
- 2) A trilevel stochastic-robust formulation is developed to

ascertain the profitability of NHEMP, where the refueling demand is modeled by DDU sets, while the other DIU factors (i.e., intermittent RES outputs and invariant electric loads) are represented by a series of scenarios.

- 3) To overcome the computational challenges associated with the stochastic-robust program with DDU, a PC&CG-based adaptive decomposition algorithm is customized and implemented that guarantees to generate an exact solution.
- 4) Numerical results demonstrate the value of DIE, the flexibility of DDU modeling, as well as the strong solution capacity of the customized PC&CG-based adaptive decomposition algorithm.

The remainder of this paper is organized as follows. Section II proposes a trilevel stochastic-robust formulation of NHEMP considering DDU of refueling demand. Section III customizes a solution method based on PC&CG. Then, we carry out case studies in Section IV to substantiate the effectiveness of our NHEMP model and customized PC&CG algorithm. Finally, in Section V, some conclusions are drawn and discussed.

II. PROBLEM FORMULATION

The model adopted is driven by the goal to deploy networked HE microgrids (as in Ref. [13]) in a carbon-free town. The supporting PDN is with a radial topology, where \mathcal{N} and \mathcal{L} denote the sets of distribution nodes and lines, respectively. The medium-voltage (MV) substation, connected to the utility grid, is located at node 0. Due to geographical and architectural restrictions, only nodes in $\Lambda \subseteq \mathcal{N}^+ = \{1, 2, \dots\}$ will be the candidates for possible deployment of HE microgrids.

A. Trilevel Stochastic-Robust NHEMP Problem with DDU

The NHEMP problem with induced refueling demand of HVs can be formulated as the following trilevel stochastic-robust program with DDU. Its target is to minimize the annualized system expenses (ASEs) under the “worst” refueling distribution by choosing the optimal siting and sizing decisions of HE microgrids.

$$\min \sum_{i \in \Lambda} \left(c_{\text{hem}}^{\text{i\&m}} u_i + \sum_{k \in \Omega_{\text{res}} \cup \Omega_{\text{ess}} \cup \Omega_{\text{hss}}} c_k^{\text{i\&m}} \bar{P}_k x_{k,i} + c_{\text{hd}}^{\text{i\&m}} n_i \right) + \sum_{s \in \mathcal{S}} \pi_s \max_{\xi_z^{s,t} \in \Xi(n_i)} \min Q_s(x_{k,i}, n_i, \xi_z^{s,t}) \quad (1)$$

$$\text{s.t.} \sum_{i \in \Lambda_z} u_i = 1, \quad \forall z \in \mathcal{Z} \quad (2)$$

$$x_{k,i}^{\min} u_i \leq x_{k,i} \leq x_{k,i}^{\max} u_i, \quad \forall k \in \Omega_{\text{res}} \cup \Omega_{\text{ess}} \cup \Omega_{\text{hss}}, \forall i \in \Lambda \quad (3)$$

$$n_i^{\min} u_i \leq n_i \leq n_i^{\max} u_i, \quad \forall i \in \Lambda \quad (4)$$

$$(6) - (32)$$

1) *Upper-Level Problem:* By choosing the optimal siting and sizing decisions for HE microgrids, the objective of the upper-level problem is to minimize the annualized summation of CAPEXs as well as the basic maintenance costs (Line 1 of (1)). We partition the town into several mutually disjoint

refueling zones. Let Λ_z denote the set of candidate nodes that can be deployed with HE microgrids in zone z . To satisfy the hydrogen supply to the local area, (2) indicates that one microgrid must be constructed in each zone. Besides, (3) and (4) show the capacity constraints for HE microgrids.

2) *Lower-Level Problem*: The objective of the lower-level problem is to minimize the operational expenses (OPEXs), i.e., power and hydrogen procurement costs, and penalty costs associated with unmet electric demand, less the revenues, as in (5). A set of stochastic scenarios ($s \in \mathcal{S}$) with probability π_s ($\sum_{s \in \mathcal{S}} \pi_s = 1$), including random variation of RES outputs ($\delta_{k,i}^{s,t}$) and uncertain electric loads ($PD_i^{s,t}$), are applied to describe the operational risks of HE microgrids. Specifically, for each scenario s , a branch of the lower-level problem is modeled as below:

$$Q_s(x_{k,i}, n_i, \zeta_z^{s,t}) = \sigma \sum_{t \in \mathcal{T}} \left[\varrho_{\text{imp}}^t p_{\text{mv}}^{s,t} + \varrho_g \sum_{i \in \Lambda} g_{\text{pur},i}^t \right] \Delta t + \sigma \sum_{t \in \mathcal{T}} \left[\iota_{\text{pl}} \sum_{i \in \mathcal{N}^+} l_i^{s,t} - \rho_e \sum_{i \in \mathcal{N}^+} p_i^{s,t} - \rho_g \sum_{i \in \Lambda} g_i^{s,t} \right] \Delta t \quad (5)$$

• *Constraints of Electrical Subsystems*: The varying RES outputs are constrained by (6) and (7). (8)-(11) are general operational constraints for electrical storage systems (ESSs), e.g., battery banks (BBs). The charging and discharging power are restricted by (8). The state-of-charge (SOC) is described by (9)-(11). Note that (11) illustrates that the net charging capacities of ESSs should be zero after a daily charging-discharging cycle [24]. (12) and (13) represent, respectively, the active and reactive power balance within each HE microgrid. Moreover, (16) is the capacity constraint for low-voltage (LV) substations, which can be linearized by the technique in Ref. [25].

$$0 \leq p_{k,i}^{s,t} \leq \delta_{k,i}^{s,t} \bar{P}_k x_{k,i}, \quad \forall k \in \Omega_{\text{res}}, \forall i \in \Lambda, \quad \forall s \in \mathcal{S}, \forall t \in \mathcal{T} \quad (6)$$

$$p_{k,i}^{s,t} \tan \varphi_k^{\min} \leq q_{k,i}^{s,t} \leq p_{k,i}^{s,t} \tan \varphi_k^{\max}, \quad \forall k \in \Omega_{\text{res}}, \forall i \in \Lambda, \forall s, \forall t \quad (7)$$

$$0 \leq pc_{k,i}^{s,t}, pd_{k,i}^{s,t} \leq \bar{P}_k x_{k,i}, \quad \forall k \in \Omega_{\text{ess}}, \forall i \in \Lambda, \forall s, \forall t \quad (8)$$

$$soc_{k,i}^{s,t+1} = soc_{k,i}^{s,t} + \left(pc_{k,i}^{s,t} \eta_k^{\text{ch}} - pd_{k,i}^{s,t} / \eta_k^{\text{dis}} \right) \Delta t, \quad \forall k \in \Omega_{\text{ess}}, \forall i \in \Lambda, \forall s, \forall t \quad (9)$$

$$(1 - DoD_k) \bar{E}_k x_{k,i} \leq soc_{k,i}^{s,t} \leq \bar{E}_k x_{k,i}, \quad \forall k \in \Omega_{\text{ess}}, \forall i \in \Lambda, \forall s, \forall t \quad (10)$$

$$\sum_{t \in \mathcal{T}} \left(pc_{k,i}^{s,t} \eta_k^{\text{ch}} - pd_{k,i}^{s,t} / \eta_k^{\text{dis}} \right) = 0, \quad \forall k \in \Omega_{\text{ess}}, \forall i \in \Lambda, \forall s, \forall t \quad (11)$$

$$\sum_{k \in \Omega_{\text{res}}} p_{k,i}^{s,t} + \sum_{k \in \Omega_{\text{ess}}} \left(pd_{k,i}^{s,t} - pc_{k,i}^{s,t} \right) + p_{\text{lv},i}^{s,t} = p_i^{s,t} + p_{\text{elz},i}^{s,t}, \quad \forall i \in \Lambda, \forall s, \forall t \quad (12)$$

$$\sum_{k \in \Omega_{\text{res}}} q_{k,i}^{s,t} + q_{\text{lv},i}^{s,t} = p_i^{s,t} \tan \varphi_{\text{pl},i}^{s,t}, \quad \forall i \in \Lambda, \forall s, \forall t \quad (13)$$

$$p_i^{s,t} + l_i^{s,t} = PD_i^{s,t}, \quad \forall i \in \mathcal{N}^+, \forall s, \forall t \quad (14)$$

$$0 \leq p_i^{s,t}, l_i^{s,t} \leq PD_i^{s,t}, \quad \forall i \in \mathcal{N}^+, \forall s, \forall t \quad (15)$$

$$\left(p_{\text{lv},i}^{s,t} \right)^2 + \left(q_{\text{lv},i}^{s,t} \right)^2 \leq \left(S_{\text{lv},i}^{\max} \right)^2, \quad \forall i \in \Lambda, \forall s, \forall t \quad (16)$$

• *Constraints of Hydrogen Subsystems*: Electrolyzers (ELZs) and hydrogen tanks (HTs) constitute the hydrogen storage system (HSS). (17) below captures the electricity-hydrogen transition process of ELZs, and (18) describes the limit on hydrogen production. (19) describes the massive balance of HTs, taking into account the dissipation factor ϕ_{ht} . The hydrogen purchased from the local hydrogen market is constrained by (20). The capacity limitation of HTs is given in (21). Combining the aggregation factor ξ_z^t , the met ($gl_i^{s,t}$) and unmet ($ul_z^{s,t}$) refueling demand of HVs are governed by (22) and (23), and $gl_i^{s,t}$ is also constrained by (24) due to the service rate (SR) of hydrogen dispensers (HDs).

$$g_{\text{elz},i}^{s,t} = \frac{\eta_{\text{elz}} p_{\text{elz},i}^{s,t}}{LHV_{\text{H}_2}}, \quad \forall i \in \Lambda, \forall s, \forall t \quad (17)$$

$$0 \leq p_{\text{elz},i}^{s,t} \leq \bar{P}_{\text{elz}} x_{\text{elz},i}, \quad \forall i \in \Lambda, \forall s, \forall t \quad (18)$$

$$loh_{\text{ht},i}^{s,t+1} = loh_{\text{ht},i}^{s,t} (1 - \phi_{\text{ht}}) + \left(g_{\text{elz},i}^{s,t} + g_{\text{pur},i}^{s,t} - gl_i^{s,t} \right) \Delta t, \quad \forall i \in \Lambda, \forall s, \forall t \quad (19)$$

$$0 \leq g_{\text{pur},i}^{s,t} \leq \bar{G}_{\text{pur},z}^t u_i, \quad \forall i \in \Lambda_z, z \in \mathcal{Z}, \forall s, \forall t \quad (20)$$

$$0 \leq loh_{\text{ht},i}^{s,t} \leq \bar{P}_{\text{ht}} x_{\text{ht},i}, \quad \forall i \in \Lambda, \forall s, \forall t \quad (21)$$

$$\sum_{i \in \Lambda_z} gl_i^{s,t} + ul_z^{s,t} = \xi_z^{s,t}, \quad \forall z \in \mathcal{Z}, \forall s, \forall t \quad (22)$$

$$0 \leq gl_i^{s,t}, ul_z^{s,t} \leq \xi_z^{s,t}, \quad \forall i \in \Lambda_z, z \in \mathcal{Z}, \forall s, \forall t \quad (23)$$

$$0 \leq gl_i^{s,t} \leq SR \cdot n_i, \quad \forall i \in \Lambda, \forall s, \forall t \quad (24)$$

• *Constraints of PDN*: The operation of PDN is described by the linearized Disflow model, as in (25)-(32). By integrating multiple HE microgrids, the nodal power balance satisfies (25)-(28). (29) is the capacity limit of distribution lines. (30) provides a bridge between the nodal voltage and distributed power, which is in the spirit of Ohm's Law [26]. The security range of voltage deviation is constrained by (31). In (32), the exchange power through the middle-voltage (MV) substation is limited by the transactive capacity. Similar to (16), the quadratic constraints (29) and (32) can also be linearized.

$$fp_{ji}^{s,t} - \sum_{l \in \mathcal{C}(i)} fp_{il}^{s,t} = \begin{cases} p_{\text{lv},i}^{s,t}, & \forall i \in \Lambda, \forall s, \forall t \\ p_i^{s,t}, & \forall i \in \mathcal{N}^+ \setminus \Lambda, \forall s, \forall t \end{cases} \quad (25)$$

$$fq_{ji}^{s,t} - \sum_{l \in \mathcal{C}(i)} fq_{il}^{s,t} = \begin{cases} q_{\text{lv},i}^{s,t}, & \forall i \in \Lambda, \forall s, \forall t \\ p_i^{s,t} \tan \varphi_{\text{pl},i}^{s,t}, & \forall i \in \mathcal{N}^+ \setminus \Lambda, \forall s, \forall t \end{cases} \quad (26)$$

$$\sum_{l \in \mathcal{C}(0)} fp_{0l}^{s,t} = p_{\text{mv}}^{s,t} \geq 0, \quad \forall s, \forall t \quad (27)$$

$$\sum_{l \in \mathcal{C}(0)} fq_{0l}^{s,t} = q_{\text{mv}}^{s,t} \geq 0, \quad \forall s, \forall t \quad (28)$$

$$\left(fp_{ij}^{s,t} \right)^2 + \left(fq_{ij}^{s,t} \right)^2 \leq \left(S_{ij}^{s,t} \right)^2, \quad \forall (i,j) \in \mathcal{L}, \forall s, \forall t \quad (29)$$

$$U_i^{s,t} - U_j^{s,t} = (r_{ij} fp_{ij}^{s,t} + x_{ij} fq_{ij}^{s,t}) / U_0, \quad \forall (i,j) \in \mathcal{L}, \forall s, \forall t \quad (30)$$

$$U_i^{\min} \leq U_i^{s,t} \leq U_i^{\max}, \quad \forall i \in \mathcal{N}, \forall s, \forall t \quad (31)$$

$$\left(p_{\text{mv}}^{s,t} \right)^2 + \left(q_{\text{mv}}^{s,t} \right)^2 \leq \left(S_{\text{mv}}^{\max} \right)^2, \quad \forall s, \forall t \quad (32)$$

3) *Middle-Level Problem*: It is essential to know whether the siting and sizing decisions are profitable enough with

the uncertainty in refueling demand. Hence, the middle-level problem focuses on identifying the “worst” refueling demand, and serves as a maximization problem. For each scenario s , we adopt a DDU set, as shown in (33)-(36), to model the refueling demand ($\xi_z^{s,t}$). (33) and (34) respectively define the upper and lower bounds on $\xi_z^{s,t}$, where $\bar{\xi}_z^{s,t}$ and $\underline{\xi}_z^{s,t}$ represent the basic bounds, and induced coefficients $\bar{\gamma}_z^t$ and $\underline{\gamma}_z^t$ are introduced to reflect DIE in each zone. The number of HDs, whose information is available to HV drivers through the transportation information system (TIS), is chosen as the representative of microgrid refueling capacities. The DDU set establishes a relationship between refueling demand and the number of HDs, rendering the bounds of $\xi_z^{s,t}$ increase with $\sum_{i \in \Lambda_z} n_i$. Besides, to avoid over conservativeness, the budget constraints, which are also decision-dependent, are included as (35) and (36). The meanings of $\bar{\zeta}^{s,t}/\underline{\zeta}^{s,t}$ and $\bar{\alpha}^t/\underline{\alpha}^t$ are analogous to those of $\bar{\xi}_z^{s,t}/\underline{\xi}_z^{s,t}$ and $\bar{\gamma}_z^t/\underline{\gamma}_z^t$, with the exception that they shift the perspective from a specific zone to encompassing the entire town.

$$\begin{aligned} \Xi^s(n_i) &= \left\{ \xi_z^{s,t} \geq 0 \mid \xi_z^{s,t} \leq \bar{\xi}_z^{s,t} + \bar{\gamma}_z^t \sum_{i \in \Lambda_z} n_i, \forall z, \forall t; \right. & (33) \\ &\quad \xi_z^{s,t} \geq \underline{\xi}_z^{s,t} + \underline{\gamma}_z^t \sum_{i \in \Lambda_z} n_i, \quad \forall z, \forall t; & (34) \\ &\quad \sum_{z \in \mathcal{Z}} \xi_z^{s,t} \leq \bar{\zeta}^{s,t} + \bar{\alpha}^t \sum_{i \in \Lambda} n_i, \quad \forall t; & (35) \\ &\quad \left. \sum_{z \in \mathcal{Z}} \xi_z^{s,t} \geq \underline{\zeta}^{s,t} + \underline{\alpha}^t \sum_{i \in \Lambda} n_i, \quad \forall t \right\} & (36) \end{aligned}$$

Fig. 2 provides an example for further illustration of the DDU set. Feasible regions of DDU and DIU sets are built by solid and dashed lines, respectively. Due to DIE, all bounds of the DDU set see an increase compared to those of the DIU one. If the DIU set is adopted for planning decisions, the derived solution may seriously underperform with respect to the investment based on the DDU set, since the former one fails to take advantage of the profitability associated with DIE.

Remark 1. If $\bar{\gamma}_z^t = \underline{\gamma}_z^t = \bar{\alpha}^t = \underline{\alpha}^t = 0$, $\Xi^s(n_i)$ will reduce to a static DIU set. Hence, the traditional DIU model is a special case of the proposed DDU one. In this regard, the properties and solution method presented in this paper are also applicable to the static trilevel DIU problem.

B. Compact Formulation

For the sake of compactness, and without any loss of generality, we express the NHEMP problem in (1)-(36) in matrix form as **DDU-NHEMP** below:

DDU – NHEMP :

$$\Phi = \min_{\mathbf{x} \in \mathcal{X}} \mathbf{c}^T \mathbf{x} + \sum_{s \in \mathcal{S}} \pi_s \max_{\xi_s \in \Xi_s(\mathbf{x})} \min_{\mathbf{y}_s \in \mathcal{Y}_s(\mathbf{x}, \xi_s)} \mathbf{d}_s^T \mathbf{y}_s \quad (37)$$

where

$$\mathcal{X} = \{ \mathbf{x} \in \{0, 1\}^{n_{x1}} \times \mathbb{N}^{n_{x2}} \mid \mathbf{A}\mathbf{x} \leq \mathbf{b} \}, \quad (38)$$

$$\Xi_s(\mathbf{x}) = \{ \xi_s \in \mathbb{R}_+^{n_\xi} \mid \mathbf{H}_s \xi_s \leq \mathbf{h}_s - \mathbf{F}_s \mathbf{x} \}, \quad (39)$$

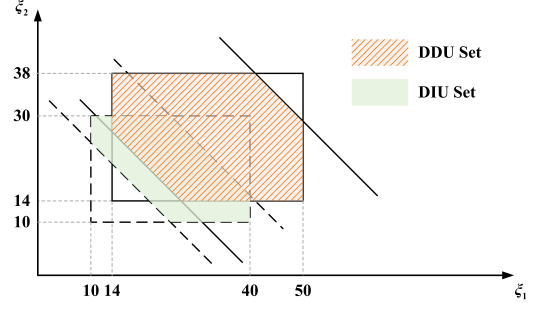


Fig. 2. Illustration of the decision-dependent uncertainty set. (Without loss of generality, indices s and t are omitted, and $|\mathcal{Z}| = 2$. Then, $\xi_1, \bar{\xi}_1, \underline{\gamma}_1, \bar{\gamma}_1, \xi_2, \bar{\xi}_2, \underline{\gamma}_2, \bar{\gamma}_2, \zeta, \bar{\zeta}, \alpha$ and $\bar{\alpha}$ are set to 10, 40, 2, 5, 10, 30, 4, 8, 35, 55, 2 and 8, respectively. Besides, $\sum_{i \in \Lambda_1} n_i = 2$ and $\sum_{i \in \Lambda_2} n_i = 1$.)

$$\mathcal{Y}_s(\mathbf{x}, \xi_s) = \{ \mathbf{y}_s \in \mathbb{R}_+^{n_y} \mid \mathbf{B}_s \mathbf{y}_s \geq \mathbf{f}_s - \mathbf{G}_s \mathbf{x} - \mathbf{E}_s \xi_s \}. \quad (40)$$

In **DDU-NHEMP**, the objective function is abstracted from (1) and (5). \mathbf{x} denotes the first-stage decisions for HE microgrids' investment strategies, \mathbf{y}_s represents the operation-related recourse decisions of scenario s , and ξ_s expresses the associated DDU parameters in the middle-level. Defined by constraints (2)-(4), \mathcal{X} indicates the feasible set of \mathbf{x} . $\Xi(\mathbf{x})$ is the DDU set as exhibited in (33)-(36), which is dependent on \mathbf{x} . Further, corresponding to (6)-(32), $\mathcal{Y}_s(\mathbf{x}, \xi_s)$ shows the feasible region of \mathbf{y}_s . n_{x1}/n_{x2} , n_ξ and n_y are proper numbers standing for dimensions of \mathbf{x} , \mathbf{y}_s and ξ_s . Moreover, we use m_ξ and m_y to denote the numbers of constraints of $\Xi_s(\mathbf{x})$ and $\mathcal{Y}_s(\mathbf{x}, \xi_s)$, respectively.

C. Some Structural Properties

1) *Relatively Complete Recourse:* **DDU-NHEMP** possesses the *relatively complete recourse*, i.e., for $s \in \mathcal{S}$, given any $\hat{\mathbf{x}} \in \mathcal{X}$ and $\hat{\xi}_s \in \Xi_s(\hat{\mathbf{x}})$, there exists feasible \mathbf{y}_s such that $\mathbf{y}_s \in \mathcal{Y}_s(\hat{\mathbf{x}}, \hat{\xi}_s)$, and the optimal value of $\min_{\mathbf{y}_s \in \mathcal{Y}_s(\hat{\mathbf{x}}, \hat{\xi}_s)} \mathbf{d}_s^T \mathbf{y}_s$ is finite. This is achieved due to the inclusion of auxiliary variables $gl_i^{s,t}$ and $pl_i^{s,t}$.

2) *Definition of \mathcal{OU}_s :* For a given $\mathbf{x} \in \mathcal{X}$, the $\max_{\xi_s \in \Xi_s(\mathbf{x})} \min_{\mathbf{y}_s \in \mathcal{Y}_s(\mathbf{x}, \xi_s)} \mathbf{d}_s^T \mathbf{y}_s$ corresponding to each scenario $s \in \mathcal{S}$ can be converted to the following single-level problem through the dual theory:

$$\max_{\xi_s \in \Xi_s(\mathbf{x}), \lambda_s \in \Pi_s} (\mathbf{f}_s - \mathbf{G}_s \mathbf{x} - \mathbf{E}_s \xi_s)^T \lambda_s, \quad \forall s \in \mathcal{S}, \quad (41)$$

where $\lambda_s \geq \mathbf{0}$ is the multiplier of (40), and its feasible set Π_s is defined as:

$$\Pi_s = \{ \lambda_s \in \mathbb{R}_+^{m_y} \mid \mathbf{d}_s - \mathbf{B}_s^T \lambda_s \geq \mathbf{0} \}. \quad (42)$$

Note that problem (41) is a bilinear program. By alternately fixing ξ_s and λ_s and leveraging the property of linear programs (LPs) [27], a non-trivial proposition can be obtained:

Proposition 1. For given $\mathbf{x} \in \mathcal{X}$ and $s \in \mathcal{S}$, when (41) reaches its optimum, there exist optimal $\hat{\xi}_s$ and $\hat{\lambda}_s$ being one of the extreme points of $\Xi_s(\mathbf{x})$ and Π_s , respectively. And $\hat{\xi}_s$ is also an optimal solution of $\max_{\xi_s \in \Xi_s(\mathbf{x})} \min_{\mathbf{y}_s \in \mathcal{Y}_s(\mathbf{x}, \xi_s)} \mathbf{d}_s^T \mathbf{y}_s$.

Different from $\Xi_s(x)$, Π_s is a fixed polyhedron that is independent of x . With a given $\lambda_s \in \Pi_s$, the optimal ξ_s of problem (41) can be obtained by solving the following LP:

$$\Psi_s(x, \lambda_s) : \max_{\xi_s \in \Xi_s(x)} (-E_s \xi_s)^T \lambda_s. \quad (43)$$

By resorting to its Karush–Kuhn–Tucker (KKT) conditions [28], the solution set of $\Psi_s(x, \lambda_s)$ can be defined as:

$$\mathcal{OU}_s(x, \lambda_s) = \left\{ \xi_s \in \mathbb{R}_+^{n_\xi}, \vartheta_s \in \mathbb{R}_+^{m_\xi} \mid H_s \xi_s \leq h_s - F_s x, (44) \right.$$

$$H_s^T \vartheta_s + E_s^T \lambda_s \geq 0, \quad (45)$$

$$\vartheta_s \circ (h_s - F_s x - H_s \xi_s) = 0, \quad (46)$$

$$\xi_s \circ (H_s^T \vartheta_s + E_s^T \lambda_s) = 0 \left. \right\}, \quad (47)$$

where ϑ_s is the corresponding multiplier of (39), and \circ denotes the Hadamard product.

DDU-NHEMP holds a trilevel min – max – min structure. Nevertheless, the traditional C&CG method [23], a recognized algorithm developed for this type of problems with DIU sets, cannot handle it. Since the DDU set $\Xi_s(x)$ varies with x dynamically, the “worst” extreme point of $\Xi_s(x^1)$ derived from x^1 will generally not be an extreme point of $\Xi_s(x^2)$ when $x^1 \neq x^2$, or even may not belong to $\Xi_s(x^2)$. Hence, it requires to further develop an adaptive algorithm to deal with this challenging problem efficiently.

III. PARAMETRIC COLUMN-AND-CONSTRAINT GENERATION ALGORITHM

In this section, we introduce and tailor the PC&CG algorithm [18], which is an advanced and exact decomposition method suitable for DDU problems with a min – max – min structure, to cope with the **DDU-NHEMP** problem.

A. Equivalent Single-Level Reformulation

For each $s \in \mathcal{S}$, let \mathcal{P}_s be the set of extreme points of Π_s . Note that \mathcal{P}_s is also independent of x . By enumerating λ_s in \mathcal{P}_s , an equivalent single-level reformulation of **DDU-NHEMP** (termed **DDU-Single**) is presented in Theorem 1, which extends the result in [18] to multiple DDU sets defined with respect to $|\mathcal{S}|$ scenarios.

Theorem 1. *DDU-NHEMP is equivalent to the following single-level mixed-integer program (MIP):*

DDU – Single :

$$\min c^T x + \sum_{s \in \mathcal{S}} \pi_s \eta_s \quad (48)$$

$$\text{s.t. } Ax \leq b \quad (49)$$

$$\eta_s \geq d_s^T y_s^{\lambda_s}, \quad \lambda_s \in \mathcal{P}_s; s \in \mathcal{S} \quad (50)$$

$$B_s y_s^{\lambda_s} \geq f_s - G_s x - E_s \xi_s^{\lambda_s}, \quad \lambda_s \in \mathcal{P}_s; s \in \mathcal{S} \quad (51)$$

$$(\xi_s^{\lambda_s}, \vartheta_s^{\lambda_s}) \in \mathcal{OU}_s(x, \lambda_s), \quad \lambda_s \in \mathcal{P}_s; s \in \mathcal{S} \quad (52)$$

$$x \in \{0, 1\}^{n_{x1}} \times \mathbb{N}^{n_{x2}}, y_s^{\lambda_s} \in \mathbb{R}_+^{n_y}, \quad (53)$$

where superscript λ_s is used to make a distinction between variables corresponding to different λ_s .

Proof. See its proof in Appendix A. \square

Actually, $\sum_{s \in \mathcal{S}} |\mathcal{P}_s|$ could be very large, rendering it impractical to solve **DDU-Single** directly. A promising scheme, which is also the main idea behind PC&CG, is to conduct computation upon subsets of \mathcal{P}_s ($s \in \mathcal{S}$), followed by gradually generating \mathcal{OU}_s sets and introducing corresponding variables and constraints to improve the solution.

B. PC&CG Decomposition

PC&CG decomposition follows a master-subproblem architecture, iteratively processing until satisfying the convergence criteria. In each iteration, PC&CG begins with a master problem (**MP**) as in (54)–(59), which is a relaxation of **DDU-Single** built on subsets $\hat{\mathcal{P}}_s$ of \mathcal{P}_s .

$$\text{MP} : \min c^T x + \sum_{s \in \mathcal{S}} \pi_s \eta_s \quad (54)$$

$$\text{s.t. } Ax \leq b \quad (55)$$

$$\eta_s \geq d_s^T y_s^{\lambda_s}, \quad \lambda_s \in \hat{\mathcal{P}}_s; s \in \mathcal{S} \quad (56)$$

$$B_s y_s^{\lambda_s} \geq f_s - G_s x - E_s \xi_s^{\lambda_s}, \quad \lambda_s \in \hat{\mathcal{P}}_s; s \in \mathcal{S} \quad (57)$$

$$(\xi_s^{\lambda_s}, \vartheta_s^{\lambda_s}) \in \mathcal{OU}_s(x, \lambda_s), \quad \lambda_s \in \hat{\mathcal{P}}_s; s \in \mathcal{S} \quad (58)$$

$$x \in \{0, 1\}^{n_{x1}} \times \mathbb{N}^{n_{x2}}, y_s^{\lambda_s} \in \mathbb{R}_+^{n_y} \quad (59)$$

Collecting the optimal $(\hat{x}, \hat{\eta}_1, \dots, \hat{\eta}_{|\mathcal{S}|})$ from **MP**, a lower bound (LB) of **DDU-Single** can be obtained as:

$$LB = c^T \hat{x} + \sum_{s \in \mathcal{S}} \pi_s \hat{\eta}_s. \quad (60)$$

Then, $|\mathcal{S}|$ subproblems (**SP_s**) defined as below will be solved to generate new variables (corresponding to “columns”) and constraints:

$$\text{SP}_s : \max_{\xi_s \in \Xi_s(\hat{x})} \min_{y_s \in \mathcal{Y}_s(\hat{x}, \xi_s)} d_s^T y_s. \quad (61)$$

We mention that **SP_s** is a bilevel LP in the max – min form. By employing the KKT conditions of its lower-level problem, **SP_s** can be converted to a single-level problem as below:

$$\max_{\xi_s, y_s} d_s^T y_s \quad (62)$$

$$\text{s.t. } H_s \xi_s \leq h_s - F_s \hat{x} \quad (63)$$

$$B_s y_s + E_s \xi_s \geq f_s - G_s \hat{x} \quad (64)$$

$$d_s - B_s^T \lambda_s \geq 0 \quad (65)$$

$$\lambda_s \circ (B_s y_s + E_s \xi_s - f_s + G_s \hat{x}) = 0 \quad (66)$$

$$y_s \circ (d_s - B_s^T \lambda_s) = 0 \quad (67)$$

$$y_s \in \mathbb{R}_+^{n_y}, \lambda_s \in \mathbb{R}_+^{m_y}. \quad (68)$$

Remark 2. Complementary slackness conditions (46) and (47) in $\mathcal{OU}_s(x, \lambda_s)$ of **MP** and (66) and (67) of **SP_s** exhibit a bilinear structure, which can be linearized by using the so-called “big-M” method. For example, for the j -th constraint of (66), i.e.,

$$\lambda_s^j (B y_s + E \xi_s - f_s + G \hat{x})^j = 0, \quad (69)$$

it can equivalently be replaced by the following constraints:

$$\lambda_s^j \leq M w_s^j, \quad (70)$$

$$(B y_s + E \xi_s - f_s + G \hat{x})^j \leq M(1 - w_s^j), \quad (71)$$

where M is a sufficiently large number and w_s^j is a binary variable. By adopting such a method to the complementarity constraints, the resulting **MP** and **SP_s** are all mixed-integer linear programs (MILPs), which can be directly solved by off-the-shelf solvers, e.g., Gurobi or CPLEX.

By solving **SP_s**, the optimal recourse variables and corresponding extreme points $(\hat{y}_1, \hat{\lambda}_1, \dots, \hat{y}_{|S|}, \hat{\lambda}_{|S|})$ can be derived, and the upper bound (UB) of **DDU-Single** is updated:

$$UB = \min \left\{ UB, \mathbf{c}^T \hat{\mathbf{x}} + \sum_{s \in \mathcal{S}} \pi_s \mathbf{d}_s^T \hat{\mathbf{y}}_s \right\}. \quad (72)$$

Following that, we will update $\hat{\mathcal{P}}_s \leftarrow \hat{\mathcal{P}}_s \cup \{\hat{\lambda}_s\}$, create new variables $\mathbf{y}_s^{\hat{\lambda}_s}$, $\boldsymbol{\xi}_s^{\hat{\lambda}_s}$ and $\boldsymbol{\vartheta}_s^{\hat{\lambda}_s}$ (corresponding to “columns”), and add new constraints (73)-(75) as optimality cuts to **MP**.

$$\eta_s \geq \mathbf{d}_s^T \mathbf{y}_s^{\hat{\lambda}_s}, \quad s \in \mathcal{S} \quad (73)$$

$$\mathbf{B}_s \mathbf{y}_s^{\hat{\lambda}_s} \geq \mathbf{f}_s - \mathbf{G}_s \mathbf{x} - \mathbf{E}_s \boldsymbol{\xi}_s^{\hat{\lambda}_s}, \quad s \in \mathcal{S} \quad (74)$$

$$(\boldsymbol{\xi}_s^{\hat{\lambda}_s}, \boldsymbol{\vartheta}_s^{\hat{\lambda}_s}) \in \mathcal{O}U_s(\mathbf{x}, \hat{\lambda}_s), \quad s \in \mathcal{S} \quad (75)$$

Finally, the PC&CG procedure will be terminated if the relative gap $(\frac{UB-LB}{LB})$ is not larger than a tolerance level ε . The overall flow of PC&CG is described in Algorithm 1, and its finite convergence result is established following that.

Algorithm 1 Parametric Column-and-Constraint Generation

- 1: **Initialization:** Set $LB \leftarrow -\infty$, $UB \leftarrow +\infty$, $\hat{\mathcal{P}}_s \leftarrow \emptyset$;
Choose the termination gap ε .
 - 2: **while** $\frac{UB-LB}{LB} > \varepsilon$ **do**
 - 3: Solve master problem **MP** as in (54)-(59).
 - 4: **if** **MP** is infeasible **then**
 - 5: Terminate the algorithm and *report infeasibility*.
 - 6: **else**
 - 7: Derive the optimal solution $(\hat{\mathbf{x}}, \hat{\eta}_1, \dots, \hat{\eta}_{|S|})$;
 - 8: Update $LB \leftarrow \mathbf{c}^T \hat{\mathbf{x}} + \sum_{s \in \mathcal{S}} \pi_s \hat{\eta}_s$.
 - 9: **end if**
 - 10: **for** $s = 1, \dots, |S|$ **do**
 - 11: Solve subproblem **SP_s** as in (62)-(65) and (68)-(71);
 - 12: Obtain the optimal solution $(\hat{y}_1, \hat{\lambda}_1, \dots, \hat{y}_{|S|}, \hat{\lambda}_{|S|})$;
 - 13: Update $\hat{\mathcal{P}}_s \leftarrow \hat{\mathcal{P}}_s \cup \{\hat{\lambda}_s\}$; Create variables $\mathbf{y}_s^{\hat{\lambda}_s}$, $\boldsymbol{\xi}_s^{\hat{\lambda}_s}$
and $\boldsymbol{\vartheta}_s^{\hat{\lambda}_s}$; Add constraints (73)-(75) to **MP**.
 - 14: **end for**
 - 15: Update $UB \leftarrow \min \{UB, \mathbf{c}^T \hat{\mathbf{x}} + \sum_{s \in \mathcal{S}} \pi_s \mathbf{d}_s^T \hat{\mathbf{y}}_s\}$.
 - 16: **end while**
-

Theorem 2. 1) PC&CG will converge to the global optimum of **DDU-Single** in a finite number of iterations.

2) The number of iterations before PC&CG terminates is bounded by $\binom{n_\xi + m_\xi}{m_\xi}^{|S|}$, and the iteration complexity of PC&CG is $\mathcal{O}(\binom{n_\xi + m_\xi}{m_\xi}^{|S|})$.

Proof. See the detailed proof in Appendix B. \square

Remark 3. 1) Compared to the basic C&CG [23], PC&CG holds similar structures, while introducing non-trivial extreme points of $\Xi_s(\mathbf{x})$ parametrically through generating λ_s . Hence, the proposed algorithm is termed as “parametric” C&CG.

TABLE I
REFUELING DEMAND INDUCE FACTORS OF DDU SET

Coefficient	Time Period (h)					
	1-4	5-8	9-12	13-16	17-20	21-24
$\bar{\gamma}_A^t$ (kg/h)	30	40	60	60	40	30
$\underline{\gamma}_A^t$ (kg/h)	25	30	40	40	35	25
$\bar{\gamma}_B^t$ (kg/h)	25	25	45	45	35	30
$\underline{\gamma}_B^t$ (kg/h)	20	20	35	35	25	20
$\bar{\gamma}_C^t$ (kg/h)	20	30	40	40	30	20
$\underline{\gamma}_C^t$ (kg/h)	15	25	30	30	25	15

2) For each $s \in \mathcal{S}$, the corresponding **SP_s** is independent of others. Therefore, it provides us with the potential to perform parallelization in practice, so as to improve the computational performance of PC&CG.

IV. CASE STUDY

Numerical tests have been performed on a 33-bus exemplary distribution network [29] to validate the proposed **DDU-NHEMP** model and the PC&CG algorithm. For HDs, we have $c_k^{i\&m} = 29974.55\$/y$ and $SR = 108\text{kg/h}$ [30], [31]. Parameters of the remaining components, i.e., photovoltaic arrays (PVs), wind turbines (WTs), BBs, ELZs and HTs, are with the same settings as in [10]. Further, the hydrogen procurement and retail prices are taken as 8\$/kg and 9.304\$/kg, respectively [10], [32]. As in [13], PDN is partitioned into three refueling zones, termed A, B and C. Table I shows the DDU coefficients $\bar{\gamma}_z^t$ and $\underline{\gamma}_z^t$ of each zone, and we have chosen $\bar{\alpha}^t = \sum_{z \in \mathcal{Z}} \bar{\gamma}_z^t / |\mathcal{Z}|$ and $\underline{\alpha}^t = \sum_{z \in \mathcal{Z}} \underline{\gamma}_z^t / |\mathcal{Z}|$. Moreover, a hybrid Latin hypercube sampling (LHS) and k-means clustering method have been adopted for stochastic scenario generation [33].

Our tests have been implemented on a mobile workstation with Intel(R) Core(TM) i9-13900H processor and 16GB RAM. The PC&CG algorithm was implemented by using Gurobi 11.0 [34]. The “big-M”s for **MP** and **SP_s** are respectively set to 10^6 and 10^9 . The termination tolerance ε is chosen as 0.1%.

A. Results of NHEMP

Cases with the same set of three stochastic scenarios are studied below.

- *Case 1:* Deploy HE microgrids without considering DIE by employing static DIU sets for refueling demand.
- *Case 2:* Deploy HE microgrids considering DIE by employing dynamic DDU sets for refueling demand.

By comparing these two cases, we have investigated the necessity and impact of the investment-induced refueling demand in the context of NHEMP.

Fig. 3 depicts the planning results of these two cases, and the average values of nodal met refueling demand (\bar{g}_i) are also exhibited, where \bar{g}_i can be calculated by

$$\bar{g}_i = \frac{\sum_{s \in \mathcal{S}} \sum_{t \in \mathcal{T}} g_i^{s,t}}{|\mathcal{S}| |\mathcal{T}|}, \quad \forall i \in \Lambda. \quad (76)$$

It can be seen that the number of HDs are, respectively, 6 and 9 for Case 1 and Case 2, and the corresponding average met

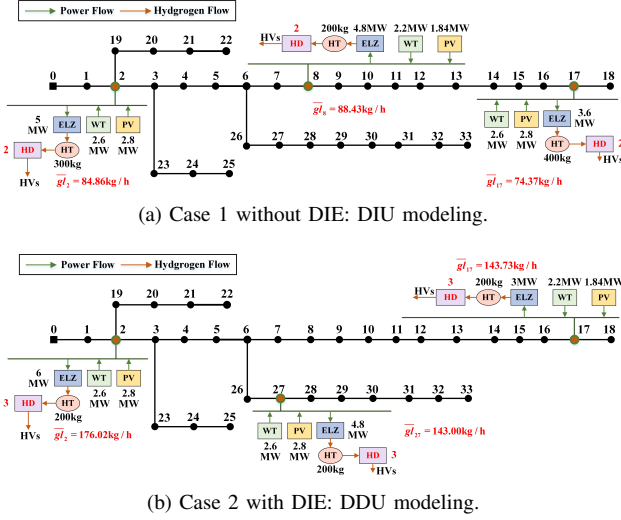


Fig. 3. Networked HE microgrids planning results.

refueling demand over the entire system (\bar{gl}), which can be defined as

$$\bar{gl} = \sum_{i \in \Lambda} \bar{gl}_i, \quad (77)$$

are 247.66kg/h and 453.75kg/h, respectively. Also, an HE microgrid at node 8 (for Case 1) is switched to node 27 (for Case 2) with a larger resource capacity. Compared to Case 1, the \bar{gl} of Case 2 has an increase of 206.09kg/h, clearly reflecting the demand-inducing effect. It can be explained that the deployment of HDs induces the growth of refueling demand, which in turn fosters the additional investments of HE microgrids. Eventually, an equilibrium state between the supply and demand sides is reached.

Next, we have investigated the economic benefits of microgrids deployment. As shown in Table II, three annualized indices, i.e., ASE (Φ), CAPEX (Φ^{capex}), and summation of OPEX and maintenance cost ($\Phi^{\text{o\&m}}$), are selected. In Case 2, Φ is -13.01 million\$, supporting the economic feasibility for investing in HE microgrids, since a negative Φ represents a positive profit over the planning scheme. Compared to Case 1, Case 2 has a 17.08% decline in $\Phi^{\text{o\&m}}$, while only with a 2.39% increase in Φ^{capex} . It shows that the DDU offers *flexibility* to NHEMP modeling. Specifically, in trilevel **DDU-NHEMP**, the middle-level problem seeks for the refueling demand as small as possible to reduce microgrid operator's revenues. With an embedded DDU set, the "worst" refueling demand will increase with the refueling capacity, thereby improving the profits. We note that Case 1# represents the expected benefits of Case 1 in an environment with DIE, which is calculated by fixing the investment decisions as the corresponding solutions to Case 1 and re-solving the DDU model. Comparing Case 1# with Case 1, the induced refueling demand is expected to result in a 1.78 million\$ decrease in Φ , suggesting that the economic benefit is underestimated if our planning results are derived by assuming a DIU set. Indeed, such an underestimation may cause us to give up an economic-feasible project in practice.

TABLE II
ECONOMIC-BENEFITS ASSESSMENT OF NHEMP

Index	Φ (million\$)	Φ^{capex} (million\$)	$\Phi^{\text{o\&m}}$ (million\$)	V_{DIE} (million\$)	\bar{V}_{DIE}
Case 1	-10.63	3.76	-14.40	\	\
Case 1#	-12.41	3.76	-16.17	\	\
Case 2	-13.01	3.85	-16.86	0.6	4.83%

To formalize our understanding, we introduce two concepts: the *Value of Demand-Inducing Effect* (V_{DIE}) and the *Relative Value of Demand-Inducing Effect* (\bar{V}_{DIE}), to quantify the change of incorporating DIE into the decision-making model. Mathematically, they are defined as:

$$V_{\text{DIE}} = \Phi_{1\#} - \Phi_2, \quad (78)$$

$$\bar{V}_{\text{DIE}} = \frac{\Phi_{1\#} - \Phi_2}{|\Phi_{1\#}|} \times 100\%, \quad (79)$$

where $\Phi_{1\#}$ and Φ_2 represent the ASE of Case 1# and Case 2, respectively. Based on their definitions and noting that the result of Case 1 is just a feasible plan for Case 2, the next result readily follows.

Proposition 2. $\Phi_{1\#} \geq \Phi_2$, i.e., $V_{\text{DIE}} \geq 0$ and $\bar{V}_{\text{DIE}} \geq 0$.

Remark 4. As shown in Table II, a 0.6 million\$ V_{DIE} and a 4.83% \bar{V}_{DIE} are reported. Actually, given that the CAPEX increase from Case 1 to Case 2 is rather marginal, which is about 0.09 million\$, we can safely attribute most of these nontrivial economic benefits to the sound investment plan derived from the DIE-aware NHEMP model. Certainly, as shown in the next subsection, the impact of DIE requires a more systematic study.

B. Sensitivity of DIE

We have further conducted sensitivity analysis of DIE based on the parameters of DDU for Case 2. For simplicity, budget constraints (35) and (36) are omitted. In the DDU set, $\bar{\gamma}_z^t$ and $\underline{\gamma}_z^t$ quantify the *unit induced capacity*. Let $\bar{\gamma}_z^t = \chi \cdot \bar{\gamma}_z^{t,0}$ and $\underline{\gamma}_z^t = \chi \cdot \underline{\gamma}_z^{t,0}$, where $\chi \in [0, 1]$, and $\bar{\gamma}_z^{t,0}$ and $\underline{\gamma}_z^{t,0}$ are the default values as in Table I. Fig. 4a depicts ASE and \bar{gl} with various χ . For \bar{gl} , it gradually increases when χ ranges from 0 to 0.5, reflecting the increase of the system refueling capacity. In this case, the marginal effect on \bar{gl} is the same (increase of 40.83kg/h per 0.1 on χ). When $\chi \geq 0.7$, \bar{gl} is nearly stable around 455.51kg/h, which mainly attributes to the system's inherent restrictions on hydrogen production, storage and refueling. On the other hand, the ASE demonstrates a negative correlation with χ decreasing from -10.21 to -13.01 million\$. The marginal value of ASE generally decreases with χ (except from 0 to 0.1). Corresponding to the growing trend of \bar{gl} , ASE experiences a rapid decline of 2.21 million\$ as χ ranges from 0 to 0.5, while for χ ranging from 0.5 to 1, the decrease in ASE is only 0.59 million\$. It suggests that as $\bar{\gamma}_z^t$ and $\underline{\gamma}_z^t$ increase, the microgrids deployment indeed achieves greater gains, but eventually some physical restrictions will impede further profitability. Moreover, Fig. 4b shows the

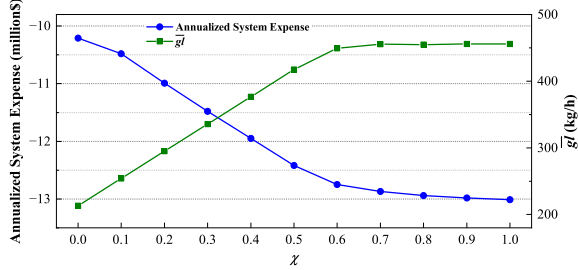
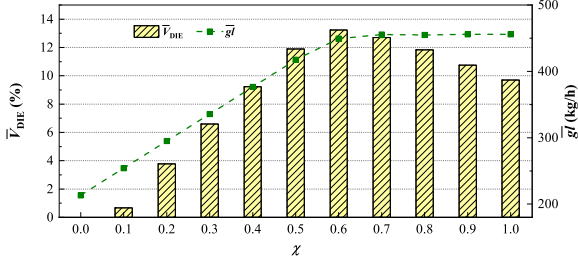
(a) Analysis of ASE and \bar{gl} .(b) Analysis of \bar{V}_{DIE} .

Fig. 4. Sensitivity of demand-inducing effect.

relationship between \bar{V}_{DIE} and χ , and the \bar{gl} curve is also given as a reference. The variation of \bar{V}_{DIE} shows an initial increase (0 to 13.23%) with χ , followed by a subsequent decrease from 13.23% to 9.70% after $\chi = 0.6$. Note that the decline emerges after \bar{gl} becomes stable. We can conclude that $\bar{\gamma}_z^t / \gamma_z^t$ positively contributes to \bar{V}_{DIE} , and this impact will be gradually reduced when other system constraints become the bottleneck.

Remark 5. Results in Fig. 4 indicate that the value of DIE are significantly influenced by the induced coefficients. Therefore, it is critical to make accurate predictions regarding $\bar{\gamma}_z^t / \gamma_z^t$, which actually are correlated with the subjective behaviors of drivers, and conduct exact numerical computation to leverage the modeling capacity of DDU, thereby unleashing the economic advantages of DIE.

C. Computational Performance of PC&CG

The computational tests of our customized PC&CG to solve different scales of **DDU-NHEMP** have been performed and analyzed.

Firstly, we have compared PC&CG with another method for the trilevel min – max – min problem with DDU, i.e., Benders C&CG (BC&CG) [18], which is basically equivalent to the modified Benders dual decomposition presented in Ref. [35]. Fig. 5 exhibits the convergence behaviors of PC&CG and BC&CG under the parameter setting in Case 2. Both of them ultimately converge to the same objective value. However, PC&CG is almost 180 times faster than BC&CG, demonstrating a clear dominance over the latter one in computational efficiency. Specifically, PC&CG could obtain initial upper and lower bounds with exceptional quality (only 2.72% gap). Then, PC&CG will quickly diminish the gap, and achieve the convergence in only 4 iterations. On the contrary, BC&CG starts with UB (-1.22×10^7) and LB (-7.68×10^{11}) with

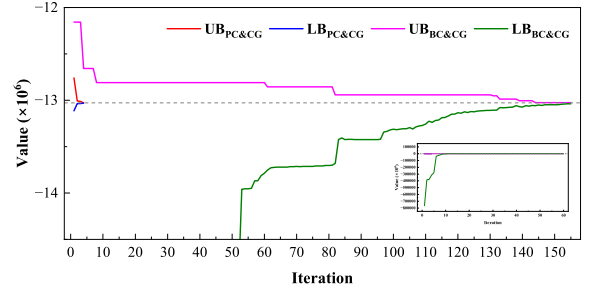


Fig. 5. Convergence behaviors of PC&CG and BC&CG. ($|\mathcal{S}| = 3$. Solution times of PC&CG and BC&CG are **41.62s** and **7410.30s**, respectively, and the corresponding numbers of iterations are **4** and **155**.)

TABLE III
COMPUTATIONAL RESULTS OF PC&CG

$ \mathcal{S} $	PC&CG				
	UB	LB	Gap	Time (s)	Iter
1	-12663447.38	-12675944.60	0.10%	5.20	2
2	-12720282.10	-12731305.32	0.09%	12.46	3
3	-13027034.59	-13030024.49	0.02%	41.62	4
4	-13583619.00	-13583619.51	<0.01%	55.68	4
5	-13600526.07	-13611305.00	0.08%	15.09	2
6	-13232295.70	-13245070.73	0.10%	38.10	3
7	-12944700.11	-12954826.34	0.08%	36.88	3
8	-12731237.61	-12731237.89	<0.01%	66.42	4
9	-12572078.93	-12575423.70	0.03%	113.70	4
10	-12348591.05	-12350884.49	0.02%	165.18	3

a very huge gap. After a few iterations from the beginning, UB and LB improve very slowly, leading to a large number of iterations before termination, thereby much longer solution time. Given the drastic difference between these two methods, we do not recommend BC&CG to compute practical instances.

Then, we have investigated the scalability of PC&CG. The computational results using PC&CG upon **DDU-NHEMP** with various numbers of scenarios ($|\mathcal{S}|$) are presented in Table III. For each instance, we show the UB and LB, relative gap (Gap), number of iterations (Iter), and computational time in seconds (Time) of PC&CG when it terminates. For all the instances with $|\mathcal{S}|$ ranging from 1 to 10, PC&CG can solve them in 4 iterations, and lead to high-quality solutions within a 0.10% gap. Even for the complex instance with 10 scenarios, it can be solved within 3 minutes. We notice that the computational time is not always increased with $|\mathcal{S}|$ monotonically (e.g., instances with $|\mathcal{S}| = 5, 6$ and 7). It also depends on the operating parameters for each scenario, which may affect the number of required iterations. Intuitively, for instances with the same number of iterations, the solution time increases with $|\mathcal{S}|$. But cases with 6 and 7 scenarios are exceptional, which spend similar amount of time for convergence. In summary, PC&CG offers a powerful and scalable computational tool to solve complex **DDU-NHEMP** problems.

V. CONCLUSION AND DISCUSSION

This paper has proposed a stochastic-robust approach to support NHEMP with DIE. A novel min – max – min formulation with DDU sets has been presented, which reflects the mutual interactions between investment decisions and HV refueling demand. To address the computational intractability, an adaptive decomposition algorithm based on PC&CG has been customized and developed. Case studies on an IEEE exemplary system have corroborated the effectiveness of our DIE-aware NHEMP model and the PC&CG algorithm. Some key observations and insights are presented as follows:

- 1) *Demand-Inducing Effect* positively contributes to the economic benefits of NHEMP; however, this impact will be gradually reduced when other system restrictions become the bottleneck.
- 2) *Decision-Dependent Uncertainty* offers a flexible modeling capacity to generate formulations. For the NHEMP problem, DDU can capture the investment induced refueling demand, and thus accurately, if solved to optimality, reflects the impact of DIE and helps us derive a sound investment plan.
- 3) *Parametric Column-and-Constraint Generation Algorithm* provides a powerful and scalable computational tool. It exactly and efficiently solves the complex trilevel stochastic-robust NHEMP problem with DDU and can be employed to solve similar types of practical problems.

APPENDIX A PROOF OF THEOREM 1

Lemma 1. For a given x and for each $s \in \mathcal{S}$,

$$\max_{\xi_s \in \Xi_s(x)} \min_{y_s \in \mathcal{Y}_s(x, \xi_s)} d^T y_s = \max_{\xi_s \in \Xi_s^*(x)} \min_{y_s \in \mathcal{Y}_s(x, \xi_s)} d^T y_s, \quad (80)$$

where $\Xi_s^*(x) = \bigcup_{\lambda_s \in \mathcal{P}_s} \mathcal{OU}_s^{\xi_s}(x, \lambda_s)$, and $\mathcal{OU}_s^{\xi_s}(x, \lambda_s)$ is the projection of $\mathcal{OU}_s(x, \lambda_s)$ onto the subspace hosting ξ_s .

Proof of Lemma 1. On the one hand, for a given $\lambda_s \in \mathcal{P}_s$, $\mathcal{OU}_s^{\xi_s}(x, \lambda_s) \subseteq \Xi_s$ holds due to the definitions of \mathcal{OU}_s and $\mathcal{OU}_s^{\xi_s}$. Hence, we have $\Xi_s^*(x) \subseteq \Xi_s$, and $LHS \geq RHS$.

On the other hand, following Proposition 1 in Section II-C, there exists an optimal $\hat{\xi}_s$ of the LHS also an optimal solution of $\Psi_s(x, \hat{\lambda}_s)$, with a certain $\hat{\lambda}_s \in \mathcal{P}_s$. Recalling the definitions of \mathcal{OU}_s and $\mathcal{OU}_s^{\xi_s}$, we have $\hat{\xi}_s \in \mathcal{OU}_s^{\xi_s}(x, \hat{\lambda}_s)$, and thus $\hat{\xi}_s \in \Xi_s^*(x)$. Hence, $LHS \leq RHS$ holds.

Together with $LHS \geq RHS$ and $LHS \leq RHS$, $LHS = RHS$ readily follows. \square

Proof of Theorem 1. Through the epigraph reformulation, **DDU-NHEMP** can be converted to

$$\min c^T x + \sum_{s \in \mathcal{S}} \pi_s \eta_s \quad (81)$$

$$\text{s.t. } x \in \mathcal{X} \quad (82)$$

$$\eta_s \geq \max_{\xi_s \in \Xi_s(x)} \min_{y_s \in \mathcal{Y}_s(x, \xi_s)} d_s^T y_s, \quad s \in \mathcal{S}. \quad (83)$$

By applying Lemma 1 and enumerating the elements of \mathcal{P}_s for every $s \in \mathcal{S}$, **DDU-Single** can be directly obtained. \square

APPENDIX B PROOF OF THEOREM 2

We introduce the standard form of $\Psi_s(x, \lambda_s)$, which can be derived by adding m_ξ non-negative slack variables:

$$\tilde{\Psi}_s(x, \lambda_s) : \min_{\tilde{\xi}_s \in \tilde{\Xi}_s(x)} \left(\tilde{E}_s \tilde{\xi}_s \right)^T \lambda_s = \mathbf{e}_s^T \tilde{\xi}_s \quad (84)$$

$$\tilde{\Xi}_s(x) = \left\{ \tilde{\xi}_s \in \mathbb{R}_+^{n_\xi + m_\xi} : \tilde{H}_s \tilde{\xi}_s = \mathbf{h}_s - F_s x \right\}. \quad (85)$$

Obviously, \tilde{H}_s is an $m_\xi \times (n_\xi + m_\xi)$ matrix, the m_ξ rows of which are linearly independent. With a $\tilde{\xi}_s$, the corresponding ξ_s can be recovered by retaining the 1-st to n_ξ -th elements of $\tilde{\xi}_s$. Note that although $\tilde{\Xi}_s(x)$ is dependent on x , the bases of \tilde{H}_s are independent of x and λ_s . Thus, the following lemma follows:

Lemma 2. For given $x' \in \mathcal{X}$ and $s \in \mathcal{S}$, consider $\tilde{\Psi}_s(x', \lambda_s)$ with a fixed λ_s . Let \mathcal{B}'_s denote a basis of \tilde{H}_s , and suppose that it corresponds to an optimal basic feasible solution (BFS) to $\tilde{\Psi}_s(x', \lambda_s)$. If the basic solution (BS) with \mathcal{B}'_s is also feasible to $\tilde{\Psi}_s(x'', \lambda_s)$, it is also optimal to $\tilde{\Psi}_s(x'', \lambda_s)$. Moreover, if \mathcal{B}'_s yields the unique optimal solution to $\tilde{\Psi}_s(x', \lambda_s)$, it also yields the unique one to $\tilde{\Psi}_s(x'', \lambda_s)$.

Proof of Lemma 2. For $s \in \mathcal{S}$, with basis \mathcal{B}'_s of \tilde{H}_s , we can reorder $\tilde{H}_s = [\mathcal{B}'_s | \mathcal{N}'_s]$ and $\mathbf{e}_s = [\mathbf{e}_{s, \mathcal{B}'_s}^T | \mathbf{e}_{s, \mathcal{N}'_s}^T]^T$. For $\tilde{\Psi}_s(x', \lambda_s)$, given the optimality of \mathcal{B}'_s , reduced cost $\mathbf{r}_{s, \mathcal{N}'_s}^T = \mathbf{e}_{s, \mathcal{N}'_s}^T - \mathbf{e}_{s, \mathcal{B}'_s}^T (\mathcal{B}'_s)^{-1} \mathcal{N}'_s \geq \mathbf{0}$. Note that $\mathbf{r}_{s, \mathcal{N}'_s}^T$ is independent of x' , i.e., $\forall x'' \in \mathcal{X}$ ($x'' \neq x'$), the inequality still holds. Hence, the BS corresponding to \mathcal{B}'_s is also optimal to $\tilde{\Psi}_s(x'', \lambda_s)$ if, and only if, it is a BFS. The second conclusion follows similarly. \square

Then, the following claim goes to support Theorem 2.

Claim 1. Let \hat{x}^τ and $(\hat{\lambda}^\tau, \dots, \hat{\lambda}_{|\mathcal{S}|}^\tau)$ be, respectively, the optimal first-stage solution and extreme points obtained in iteration τ of PC&CG, and \mathcal{B}_s^τ ($\forall s \in \mathcal{S}$) denote the basis of $\tilde{\Psi}_s(\hat{x}^\tau, \hat{\lambda}_s^\tau)$ that corresponds to an optimal BFS. For iteration τ_1 and τ_2 ($\tau_1 < \tau_2$), if $(\mathcal{B}_1^{\tau_1}, \dots, \mathcal{B}_{|\mathcal{S}|}^{\tau_1}) = (\mathcal{B}_1^{\tau_2}, \dots, \mathcal{B}_{|\mathcal{S}|}^{\tau_2})$, $UB = LB$ must hold in iteration τ_2 .

Proof of Claim 1. For a practical **DDU-NHEMP** problem, the optimal solution of $\tilde{\Psi}_s(x, \lambda_s)$ with certain x and λ_s is generally unique. In iteration τ_2 , for each $s \in \mathcal{S}$, we use $\tilde{\xi}_s^{\tau_2} = (\mathcal{B}_s^{\tau_2})^{-1}(\mathbf{h}_s - F_s \hat{x}^{\tau_2}) \geq \mathbf{0}$ denoting the unique optimal BFS to $\tilde{\Psi}_s(\hat{x}^{\tau_2}, \hat{\lambda}_s^{\tau_2})$ with $\mathcal{B}_s^{\tau_2}$, and $\tilde{\xi}_s^{\tau_2}$ being $\tilde{\xi}_s^{\tau_2}$'s incarnation in $\Xi_s(x^{\tau_2})$. Thus,

$$\max_{\xi_s \in \Xi_s(\hat{x}_2)} \min_{y_s \in \mathcal{Y}_s(\hat{x}_2, \xi_s)} d_s^T y_s = \min_{y_s \in \mathcal{Y}_s(\hat{x}_2, \hat{\xi}_s^{\tau_2})} d_s^T y_s. \quad (86)$$

Shift perspective to iteration τ_1 : Recalling the uniqueness condition, for each s , $\mathcal{B}_s^{\tau_1}$ yields the unique optimal BFS to $\tilde{\Psi}_s(\hat{x}^{\tau_1}, \hat{\lambda}_s^{\tau_1})$. Since $(\mathcal{B}_1^{\tau_1}, \dots, \mathcal{B}_{|\mathcal{S}|}^{\tau_1}) = (\mathcal{B}_1^{\tau_2}, \dots, \mathcal{B}_{|\mathcal{S}|}^{\tau_2})$, according to Lemma 2, $\mathcal{B}_s^{\tau_2}$ also yields the unique optimal BFS to $\tilde{\Psi}_s(\hat{x}^{\tau_2}, \hat{\lambda}_s^{\tau_2})$, i.e., $(\mathcal{B}_s^{\tau_2})^{-1}(\mathbf{h}_s - F_s \hat{x}^{\tau_2}) = \tilde{\xi}_s^{\tau_2}$. Hence, $\mathcal{OU}_s^{\xi_s}(\hat{x}^{\tau_2}, \hat{\lambda}_s^{\tau_1}) = \{\tilde{\xi}_s^{\tau_2}\}$.

Return to iteration τ_2 : Note that $\hat{\lambda}_s^{\tau_1} \in \hat{\mathcal{P}}_s$ ($\forall s$) exists, and thus

$$LB \geq c^T \hat{x}^{\tau_2} + \sum_{s \in \mathcal{S}} \pi_s \min \eta_s \quad (87)$$

$$\text{s.t. } \eta_s \geq d_s^T y_s^{\hat{\lambda}_s^{\tau_1}}, \quad s \in \mathcal{S} \quad (88)$$

$$B y_s^{\hat{\lambda}_s^{\tau_1}} \geq f_s - G_s x - E_s \hat{\xi}_s^{\tau_2}, \quad s \in \mathcal{S} \quad (89)$$

$$y_s^{\hat{\lambda}_s^{\tau_1}} \in \mathbb{R}_+^{n_y}, \quad s \in \mathcal{S} \quad (90)$$

$$= c^T \hat{x}^{\tau_2} + \sum_{s \in \mathcal{S}} \pi_s \max_{\xi_s \in \Xi_s(\hat{x}_2)} \min_{y_s \in \mathcal{Y}_s(\hat{x}_2, \xi_s)} d_s^T y_s \quad (91)$$

$$\geq UB. \quad (92)$$

The equality follows from (86). The second inequality holds due to the definition of UB in (72). And also, we always have $LB \leq UB$. Thus, $UB = LB$ holds.

When the uniqueness condition is not satisfied, for \mathfrak{B}_s^τ , there must exist a component j in the related reduced cost such that $(r_{s, \eta_s^\tau}^T)^j = 0$. The basic idea is to adjust $(\epsilon_s^\tau)^j$, so that $(r_{s, \eta_s^\tau}^T)^j > 0$. In this situation, the conclusion still holds following the aforementioned proof process. For more details, please refer to Ref. [18]. \square

Proof of Theorem 2. For each s , the number of bases of \widetilde{H} is finite, which is up to $\binom{n_\xi + m_\xi}{m_\xi}$. Recall the conclusion in Claim 1, that PC&CG exhibits finite convergence. With the existence of $|\mathcal{S}|$ scenarios, the iteration number before PC&CG converges is bounded by $\binom{n_\xi + m_\xi}{m_\xi}^{|\mathcal{S}|}$, and thus the iteration complexity of PC&CG is $\mathcal{O}(\binom{n_\xi + m_\xi}{m_\xi}^{|\mathcal{S}|})$. \square

REFERENCES

- [1] Intergovernmental Panel on Climate Change, "Global warming of 1.5°C," 2018. [Online]. Available: <https://www.ipcc.ch/sr15>
- [2] X. Chen *et al.*, "Pathway toward carbon-neutral electrical systems in China by mid-century with negative CO₂ abatement costs informed by high-resolution modeling," *Joule*, vol. 5, no. 10, pp. 2715–2741, 2021.
- [3] H. Zhang *et al.*, "How does load-side re-electrification help carbon neutrality in energy systems: Cost competitiveness analysis and life-cycle deduction," *Renew. Sust. Energ. Rev.*, vol. 187, p. 113745, 2023.
- [4] International Energy Agency, "The role of CCUS in low-carbon power systems," 2020. [Online]. Available: <https://www.iea.org/reports/the-role-of-ccus-in-low-carbon-power-systems>
- [5] C. Shao, K. Li, Z. Hu, and M. Shahidehpour, "Coordinated planning of electric power and natural gas distribution systems with refueling stations for alternative fuel vehicles in transportation system," *IEEE Trans. Smart Grid*, vol. 13, no. 5, pp. 3558–3569, 2022.
- [6] C. C. Chan, "The state of the art of electric, hybrid, and fuel cell vehicles," *Proc. IEEE*, vol. 95, no. 4, pp. 704–718, 2007.
- [7] T. Sinigaglia, F. Lewiski, M. E. S. Martins, and J. C. M. Siluk, "Production, storage, fuel stations of hydrogen and its utilization in automotive applications: a review," *Int. J. Hydrogen Energy*, vol. 42, no. 39, pp. 24597–24611, 2017.
- [8] P. Nikolaidis and A. Poullikkas, "A comparative overview of hydrogen production processes," *Renew. Sust. Energ. Rev.*, vol. 67, pp. 597–611, 2017.
- [9] A. M. Abdalla, S. Hossain, O. B. Nisfindy, A. T. Azad, M. Dawood, and A. K. Azad, "Hydrogen production, storage, transportation and key challenges with applications: A review," *Energy Convers. Manag.*, vol. 165, pp. 602–627, 2018.
- [10] X. Cao, X. Sun, Z. Xu, B. Zeng, and X. Guan, "Hydrogen-based networked microgrids planning through two-stage stochastic programming with mixed-integer conic recourse," *IEEE Trans. Autom. Sci. Eng.*, vol. 19, no. 4, pp. 3672–3685, 2022.
- [11] N. A. El-Taweel, H. Khani, and H. E. Z. Farag, "Hydrogen storage optimal scheduling for fuel supply and capacity-based demand response program under dynamic hydrogen pricing," *IEEE Trans. Smart Grid*, vol. 10, no. 4, pp. 4531–4542, 2019.
- [12] G. Glenk and S. Reichelstein, "Economics of converting renewable power to hydrogen," *Nat. Energy*, vol. 4, no. 3, pp. 216–222, 2019.
- [13] X. Sun, X. Cao, B. Zeng, Q. Zhai, and X. Guan, "Multistage dynamic planning of integrated hydrogen-electrical microgrids under multiscale uncertainties," *IEEE Trans. Smart Grid*, vol. 14, no. 5, pp. 3482–3498, 2023.
- [14] X. Wu, B. Cao, B. Liu, Z. Zhang, and X. Wang, "Capacity planning of carbon-free microgrid with hydrogen storage considering robust short-term off-grid operation," *Renew. Energ.*, vol. 202, pp. 242–254, 2023.
- [15] Y. Dong, W. Zheng, X. Cao, X. Sun, and Z. He, "Co-planning of hydrogen-based microgrids and fuel-cell bus operation centers under low-carbon and resilience considerations," *Appl. Energy*, vol. 336, p. 120849, 2023.
- [16] G. Pan, W. Gu, Y. Lu, H. Qiu, S. Lu, and S. Yao, "Optimal planning for electricity-hydrogen integrated energy system considering power to hydrogen and heat and seasonal storage," *IEEE Trans. Sustain. Energy*, vol. 11, no. 4, pp. 2662–2676, 2020.
- [17] L. Hellemo, P. I. Barton, and A. Tomasgard, "Decision-dependent probabilities in stochastic programs with recourse," *Comput. Manag. Sci.*, vol. 15, pp. 369–395, 2018.
- [18] B. Zeng and W. Wang, "Two-stage robust optimization with decision dependent uncertainty," *arXiv preprint arXiv:2203.16484*, 2022.
- [19] R. B. Noland and L. L. Lem, "A review of the evidence for induced travel and changes in transportation and environmental policy in the US and the UK," *Transport. Res. D-Tr. E.*, vol. 7, no. 1, pp. 1–26, 2002.
- [20] D. B. Lee Jr, L. A. Klein, and G. Camus, "Induced traffic and induced demand," *Transport. Res. Rec.*, vol. 1659, no. 1, pp. 68–75, 1999.
- [21] Ö. Mahmutoğulları and H. Yaman, "Robust alternative fuel refueling station location problem with routing under decision-dependent flow uncertainty," *Eur. J. Oper. Res.*, vol. 306, no. 1, pp. 173–188, 2023.
- [22] S. Li, L. Tong, J. Xing, and Y. Zhou, "The market for electric vehicles: Indirect network effects and policy design," *J. Assoc. Environ. Reso.*, vol. 4, no. 1, pp. 89–133, 2017.
- [23] B. Zeng and L. Zhao, "Solving two-stage robust optimization problems using a column-and-constraint generation method," *Oper. Res. Lett.*, vol. 41, no. 5, pp. 457–461, 2013.
- [24] A. Bhattacharya, J. P. Kharoufeh, and B. Zeng, "Managing energy storage in microgrids: A multistage stochastic programming approach," *IEEE Trans. Smart Grid*, vol. 9, no. 1, pp. 483–496, 2018.
- [25] X. Chen, W. Wu, B. Zhang, and C. Lin, "Data-driven DG capacity assessment method for active distribution networks," *IEEE Trans. Power Syst.*, vol. 32, no. 5, pp. 3946–3957, 2017.
- [26] M. Farivar and S. H. Low, "Branch flow model: Relaxations and convexification—Part I," *IEEE Trans. Power Syst.*, vol. 28, no. 3, pp. 2554–2564, 2013.
- [27] H. Karloff, *Linear Programming*. Springer Science & Business Media, 2008.
- [28] S. Boyd and L. Vandenberghe, *Convex Optimization*. Cambridge university press, 2004.
- [29] M. Baran and F. Wu, "Network reconfiguration in distribution systems for loss reduction and load balancing," *IEEE Trans. Power Del.*, vol. 4, no. 2, pp. 1401–1407, 1989.
- [30] California Energy Commission, "Joint Agency Staff Report on Assembly Bill 8: Assessment of Time and Cost Needed to Attain 100 Hydrogen Refueling Stations in California," 2015. [Online]. Available: https://h2fc.org/sites/default/files/CEC_ARB_Joint_Staff_Report.pdf
- [31] Y. Liu, A. Siekmann, V. Sujana, M. Uddin, F. Xie, and S. Ou, "Providing leveled cost and waiting time inputs for HDV hydrogen refueling station planning: A case study of U.S. I-75 corridor." [Online]. Available: <https://www.osti.gov/biblio/1876290>
- [32] J. Liu, Z. Xu, J. Wu, K. Liu, and X. Guan, "Optimal planning of distributed hydrogen-based multi-energy systems," *Appl. Energy*, vol. 281, p. 116107, 2021.
- [33] H. Yu, C. Y. Chung, K. P. Wong, H. W. Lee, and J. H. Zhang, "Probabilistic load flow evaluation with hybrid latin hypercube sampling and cholesky decomposition," *IEEE Trans. Power Syst.*, vol. 24, no. 2, pp. 661–667, 2009.
- [34] Gurobi Optimization, LLC, "Gurobi Optimizer Reference Manual," 2023. [Online]. Available: <https://www.gurobi.com>
- [35] Y. Zhang, F. Liu, Y. Su, Y. Chen, Z. Wang, and J. P. S. Catalão, "Two-stage robust optimization under decision dependent uncertainty," *IEEE/CAA J. Autom. Sin.*, vol. 9, no. 7, pp. 1295–1306, 2022.